Available online at www.sciencedirect.com

SciVerse ScienceDirect

journal homepage: www.elsevier.com/locate/he

Molybdenum effect on the kinetic behavior of a metal hydride electrode

Verónica Díaz [a,*], Erika Teliz [b], Fabricio Ruiz [c,d], Pablo S. Martínez [d], Ricardo Faccio [e,f,g], Fernando Zinola [b]

[a] Udelar, Facultad de Ingenieria, Instituto de Ingeniería Química, Núcleo Interdisciplinario Ingeniería Electroquímica, J. Herrera y Reisig 565, CP 11300 Montevideo, Uruguay

[b] Udelar, Facultad de Ciencias, Laboratorio de Electroquímica Fundamental, Núcleo Interdisciplinario Ingeniería Electroquímica, Igua 4225, CP 11400 Montevideo, Uruguay

[c] CONICET Consejo Nacional de Investigaciones Científicas y Técnicas, Av. Rivadavia 1917, C1033AAJ Ciudad de Buenos Aires, Argentina

[d] Centro Atómico Bariloche, Comisión Nacional de Energía Atómica (CAB-CNEA), Av. Bustillo 9500, CP 8400 S.C. de Bariloche, RN, Argentina

[e] Crystallography, Solid State and Materials Laboratory (Cryssmat-Lab), DETEMA, Facultad de Química, Universidad de la República, Montevideo, Uruguay

[f] Centro NanoMat, Polo Tecnológico de Pando, Facultad de Química, Universidad de la República, Montevideo, Uruguay

[g] Espacio Interdisciplinario, Facultad de Química, Universidad de la República, Montevideo, Uruguay

ARTICLE INFO

Article history:
Received 7 June 2013
Received in revised form
27 June 2013
Accepted 20 July 2013
Available online 16 August 2013

Keywords:
Metal hydrides
Electrochemical properties
Molybdenum
Batteries

ABSTRACT

In the present investigation, the effect of the Mo in the $LaNi_{3,6}Co_{0,7}Mn_{(0.4-x)}Al_{0,3}Mo_x$ AB5-type hydrogen storage alloys was studied. The alloys structural and microstructural characterizations were performed by means of X-ray diffraction phase analysis and scanning electron microscopy.

The electrochemical properties were studied through the measurements of discharge capacity, activation process, rate capability and electrochemical impedance spectroscopy of the electrodes.

The replacement of manganese by molybdenum, in the intermediate concentration tested (2% w/w) has a positive effect. This alloy presents the greatest discharge capacity, the closest potential to system equilibrium potential and therefore the lowest over-potentials. This alloy also has the best behavior for high-rate dischargeability and in concordance, the lowest charge transfer resistance. This improvement is thought to be due to an increase in the active area.

1. Introduction

Metal hydride alloys are mostly used as materials for negative electrodes in alkaline rechargeable cells and hydrogen storage. Nickel-metal hydride batteries are currently applied in many fields such as portable electronic devices and electric vehicles hybrid electric vehicles. These batteries depict larger gravimetric and volumetric energy densities than nickel–cadmium

* Corresponding author.
E-mail address: verodiaz@fing.edu.uy (V. Díaz).

0360-3199/$ – see front matter
http://dx.doi.org/10.1016/j.ijhydene.2013.07.079

batteries. Besides, they are friendlier towards the environment. The performance of a nickel-metal hydride battery strongly depends on the characteristics on the anode [1–8].

The investigations carried out with intermetallic AB5 alloys; seek to partially replace the constituent elements of the $LaNi_5$ compound by other chemical elements to enhance its electrochemical properties. The developed alloys, such as $LaNi_{4,8}Co_{0,5}Sn_{0,25}$, $La_{0,89}Nd_{0,2}Ni_{4,75}Co_{0,5}Sn_{0,25}$ and $La_{0,8}Ce_{0,2}Ni_{4,8}Sn_{0,25}$, which inner compositions retain lanthanum and nickel elements, are those that exhibit better behaviors. The latter presents a lower equilibrium pressure and minimum hysteresis in the curves of charge/discharge, as well as depicts a wide range of hydrogen absorption [2–9].

Recently, much more interest has grown in the study of metal hydrides based on Laves phases of zirconium, *i.e.* AB_2 type intermetallic compounds due to their greater storage capacity, and hence greater electrical charge capacity of the battery. However, its power density was not comparable to those of AB_5 type, which motivate investigation developments in order to optimize its composition [10–12].

Metal alloy plays a fundamental role in electrode processes of hydrogen absorption, defining the hydrogen reaction rate with the metal as well as the incorporation into its structure.

Different processes occur during activation [3,13–16] such as: i) reduction of surface oxides that interfere with the absorption of hydrogen, ii) reduction of the particle size due to the fractures caused by the increase in volume, iii) change in the chemical composition and/or metal surface structure [12].

Recently, AB_5 [17–21] metal hydride (MH) alloys have been intensively investigated to improve the performance of based Ni/MH batteries. Molybdenum was found to be beneficial to the low-temperature applications [22–25]. Besides, it was found that the addition of molybdenum improved the −40 °C charge efficiency through the enhancement of surface charge-transfer reaction [24]. The improvement in low-temperature performance in the molybdenum-containing AB_5 alloy was also confirmed by Iwakura et al. They connected the performance improvement of this alloy to its better bulk hydrogen diffusion and surface charge-transfer reaction [26]. Jaksic demonstrated a reduction in the hydrogen overpotential inside the alloy that had its surface being modified by galvanic codeposition of molybdenum and cobalt [27]. Furthermore, it was reported an increased hydrogen storage capacity with the substitution of nickel or cobalt by molybdenum [28,29]. Small amounts of molybdenum-substitution were found to increase the room temperature high-rate dischargeability (HRD) and surface charge-transfer current [30,31].

Although many general characteristics of molybdenum-modified AB5 alloys have been reported, a more systematic study on the influence of molybdenum to the structural and electrochemical properties is needed and will be presented in this paper.

The present study examines the electrochemical properties of the $LaNi_{3.6}Co_{0.7}Mn_{0.4}Al_{0.3}$ electrode material and their correlations with structural-microstructural characteristics. The effect of manganese substitution by molybdenum in this material is also evaluated, at room temperature, with regard to electrochemical and structural-microstructural properties.

2. Experimental

2.1. Synthesis of alloys and fabrication of negative electrodes

The alloys are prepared by arc melting adequate proportions of the composition elements (purity better than 99.9%) inside a copper-cooled hearth under high purity argon (99.998%). The alloys were remelted for the purpose of homogenization. After then, it was mechanically pulverized for the electrode formation. For the electrochemical characterization, electrodes were prepared by compacting a mixture of 50 mg of sample powders with equal amounts of teflonized carbon (Vulcan XC-72), inside a cylindrical die to a pressure of 200 MPa at room temperature, resulting the total electrode surface of 2 cm^2. A nickel wire was used as current collector. Details of electrode preparation are depicted in a previous work [9].

Three alloys were synthesized replacing manganese by molybdenum: AB_5M0 (Mo 0% w/w), AB_5M1 (Mo 2% w/w) and AB_5M2 (Mo 5% w/w).

2.2. Structural and microstructural characterization of MH electrodes

The prepared electrodes were subjected to X-ray diffraction characterization. X-ray powder diffraction data were collected for all the samples using a Rigaku ULTIMA IV, 285 mm radius, powder diffractometer operating in Bragg Brentano geometry. CuKα radiation (λ = 1.5418 Å) monochromatized with a diffracted beam bent germanium crystal was used to collect data over the 10–110° 2θ range in steps of 0.02° using a scintillation detector. Fixed slits of 1/3° were used for data collection to prevent beam spillage outside the 2 cm long sample (along the beam-path) at low angles. Peak positions were extracted from the data using the software POWDERX [32] and peak indexing and unit cell determination was performed with the software DICVOL04 [33] in order to determine the unit cell and space group symmetry of the crystalline samples.

Further analysis consisted in the full pattern profile fitting, using the Rietveld method [34] by means of the EXPGUI-GSAS suite [35,36] that allowed to extract relevant structural parameters and corresponding weight fraction in the case of multiphase systems.

Before electrochemical testing of the electrodes, the surface alloy microstructures were examined by means of a scanning electron microscope (SEM, JEOL JSM 5900) that employed a 25 kV secondary electron imaging mode.

2.3. Electrochemical characterization

We worked with AB_5-type alloys with nominal compositions AB5M0, AB5M1 and AB5M2. The hydride forming electrodes were made as it just has detailed [9]. The mixture was pressed onto a nickel mesh at room temperature. The geometrical area of the electrodes was 2 cm^2 and the thickness was around 1 mm.

Electrochemical measurements were made in a three-compartment cell with the corresponding working electrode (metal hydride electrode), counter electrode (nickel mesh) and

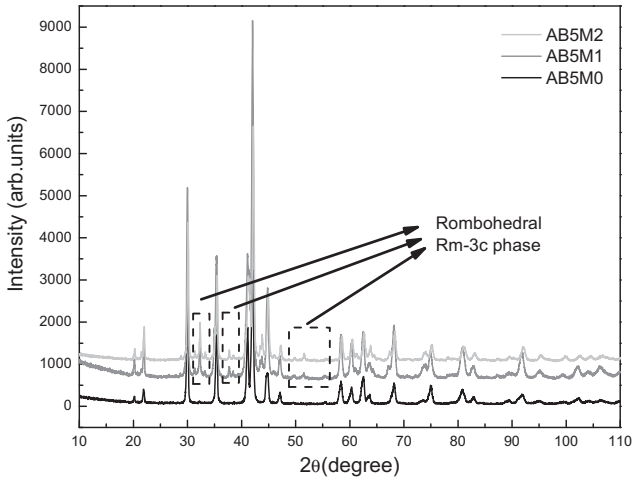

Fig. 1 – X-ray diagrams for AB5M0, AB5M1 and AB5M2 indicating the peaks corresponding to the Rhombohedral impurity.

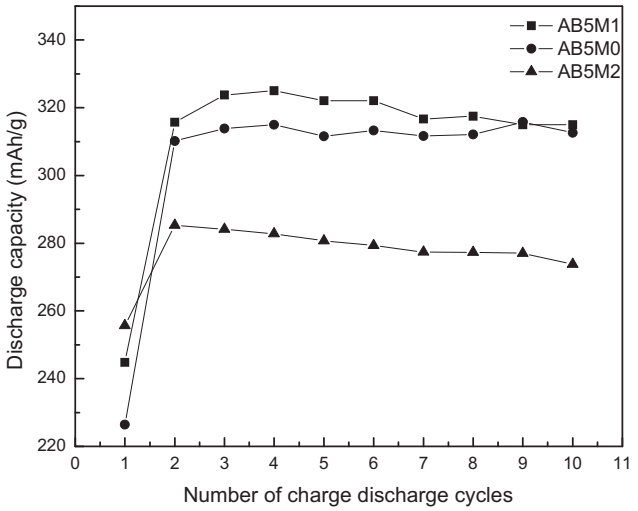

Fig. 2 – Discharge capacity of AB5M0, AB5M1 and AB5M2 alloys vs. number of charge/discharge cycles.

reference electrode (Hg/HgO electrodes). In this work potentials are referred to the Hg/HgO reference electrode. The electrolyte, 6 M KOH solution, was prepared from reagent grade KOH and Millipore-MilliQ® plus water. The experiments were carried out at room temperature. Before the electrochemical impedance spectrum (EIS) measurements, the electrodes were charge–discharge cycled at constant current for 10 cycles.

During charge–discharge experiments, constant currents of −100 mA/g and 50 mA/g respectively, were used with a charge time of 4 h and a cut off potential of −0.6 V, during discharge. After cycling the electrodes were discharged to a state of charge (SOC) of 70%, and left at open circuit potential (Eo). The EIS spectra were recorded, at Eo, in the 50 kHz–1 mHz frequency range, with a 6 mV amplitude, ten points per decade.

All the electrochemical experiments were conducted using a PGZ 301 Voltalab® potentiostat–galvanostat device. Rate capability experiments are performed at discharge charges in the range of 0.1 C–1 C.

3. Results and discussion

The XRD diagrams for AB5M0, AB5M1 and AB5M2 are presented in Fig. 1. According to this AB5M0 sample is a single phase crystalline alloy, indexed in the corresponding $CaCu_5$-type structure in the P6/mmm space group [37]. In the case of AB5M1 and AB5M2 samples there is coexistence between the $CaCu_5$-type and $CaCu_3$-type crystalline phase, the presence of the latest one is indicated in Fig. 1. According to Rietveld Refinement, the weight fractions for the Rombohedral phases correspond to 15.9% and 19.3% for AB5M1 and AB5M2 respectively.

The incorporation of a brand new molybdenum species in parent AB5M0 alloy introduces changes in the crystal structure AB5M1 and AB5M2 alloys, giving place to a net decrease in the structural cell parameters and unit cell volume of both crystalline phases, see Table 1.

It is noteworthy to mention that changes on these alloys are particularly small. In the case of P6/mmm phase, the changes corresponds to −0.039% and −0.072% for *a* and *c* unit cell parameters for AB5M1 sample when comparing to parent AB5M0 alloy. In the case of AB5M2 sample, the changes are −0.245% and −0.339% for *a* and *c* cell parameters of the hexagonal P6/mmm crystalline phases.

In conclusion, the incorporation of molybdenum induces contraction in the cell parameters of the crystalline structure of the studied alloys. This phenomenon is accompanied by a coexistence of two crystal structures, with general AB_5 and AB_3 stoichiometry.

Fig. 2 shows the discharge capacities as a function of the cycle numbers for AB5M0, AB5M1 and AB5M2 alloys. From this figure, it arises that AB5M1 depicts the highest capacity value.

Table 1 – Cell parameters, cell volume and weight fraction for the two crystalline phases.

	P6/mmm				R$\bar{3}$mH			
	a (Å)	*c* (Å)	V (Å3)	%	*a* (Å)	*c* (Å)	V (Å3)	%
AB5M0	5.06812 (25)	4.04763 (24)	90.038 (8)	100	–	–	–	–
AB5M1	5.06613 (21)	4.04470 (21)	89.932 (8)	84.1 (1)	5.1249 (5)	24.802 (4)	564.14 (11)	15.9 (2)
AB5M2	5.05569 (26)	4.03389 (26)	89.293 (9)	80.7 (3)	5.1151 (5)	24.780 (4)	561.49 (11)	19.3 (2)

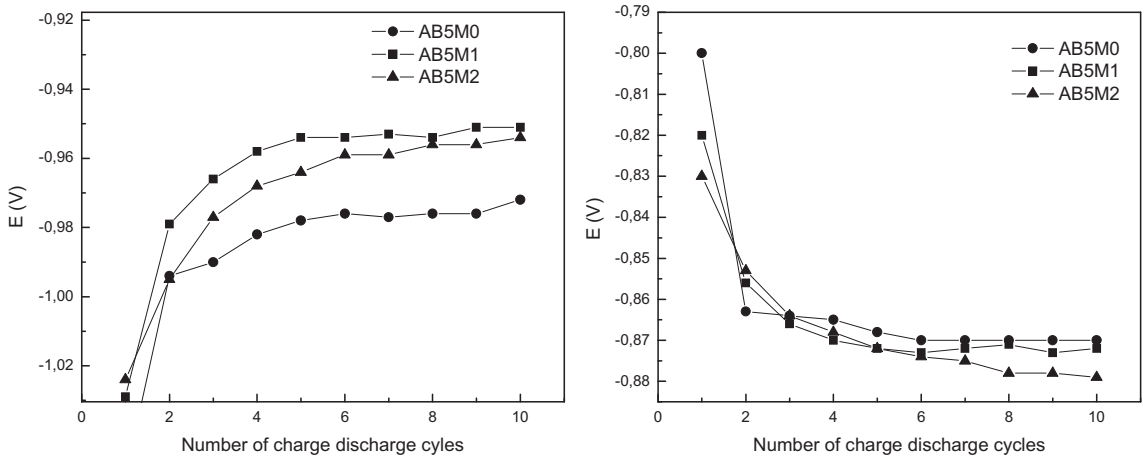

Fig. 3 – Potential values corresponding to the end of the charge process and to the half of the discharge process vs. number of charge/discharge cycles.

Moreover, the fast activation of the samples is also clearly observed. They attain the maximum capacity value approximately at the third cycle. After ten cycles AB5M0 and AB5M1 attained a similar capacity (315 mAh/g). On the other hand, AB5M2 alloy depicts after ten cycles a capacity value 13% smaller (274 mAh/g).

From potential values corresponding to the end of the charge process and to the half of the discharge process (Fig. 3), it can be seen that the AB5M1 alloy potential is the closest to the equilibrium potential of the system, this is ~0.9 V and therefore this alloy depicts the lowest overpotentials [38].

From this figure it can also be conclude that the departure from the equilibrium potential decreases with the electrochemical cycling. This behavior can be seen in all the samples. This fact could be associated with the emergence of new area as a result of particles break as a consequence of hydriding/dehydriding processes.

The high-rate dischargeability (HRD), this is, the electrochemical discharge capacity as a function of the discharge current density Id (mA/g), expressed in percent of the maximum capacity is plotted in Fig. 4. It can be observed again that M1 alloy presents the best behavior.

By increasing the discharge current, we observed a decrease in the discharge capacity due to the overpotential increase.

From the results above we can conclude a beneficial effect of the incorporation of Mo, in the sample AB5M1. This may be due to the increase in kinetic (greater i_0), the increase in the transport of material in the alloy (greater D) or to a greater pulverization of the alloy during activation (smaller particle size).

To clarify the nature of the processes that are influenced by the incorporation of Mo, EIS experiments were performed.

The EIS results (SOC 70%) are shown in the Nyquist plots in Fig. 5. It can be seen that the four studied alloys exhibit a distorted semicircle at high frequencies. This capacitive

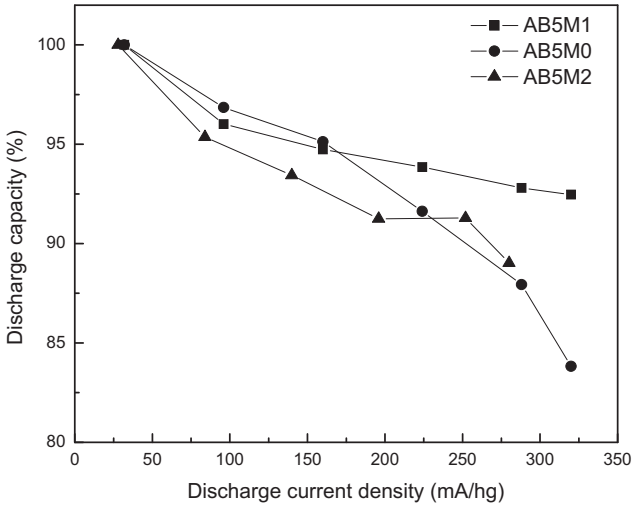

Fig. 4 – HRD, discharge capacity expressed in percent of the maximum capacity, as a function of the discharge current density.

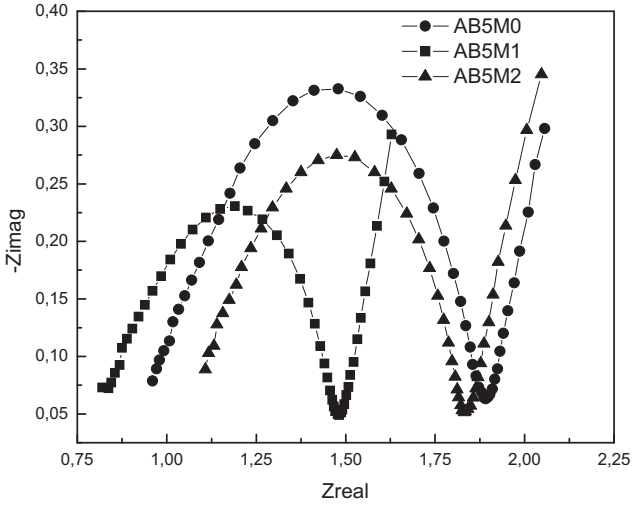

Fig. 5 – Electrochemical impedance spectra of all samples. SOC 70%.

response is associated to the relaxation of the interface capacity in parallel with the charge-transfer resistance (R_{ct}). As it can be observed, the M1 alloy exhibits the smallest semicircle diameter at high frequencies, indicating that this alloy has the lowest R_{ct} value. From the relation between R_{ct} and the exchange current density, i_0, associated to the hydriding process [39,40], it can be conclude that it has the largest value of i_0, and therefore, the best electrocatalytic properties for the hydriding process. Besides, it can also be observed at low frequencies the existence of a straight line in the Nyquist plot, associated to the hydrogen diffusion process.

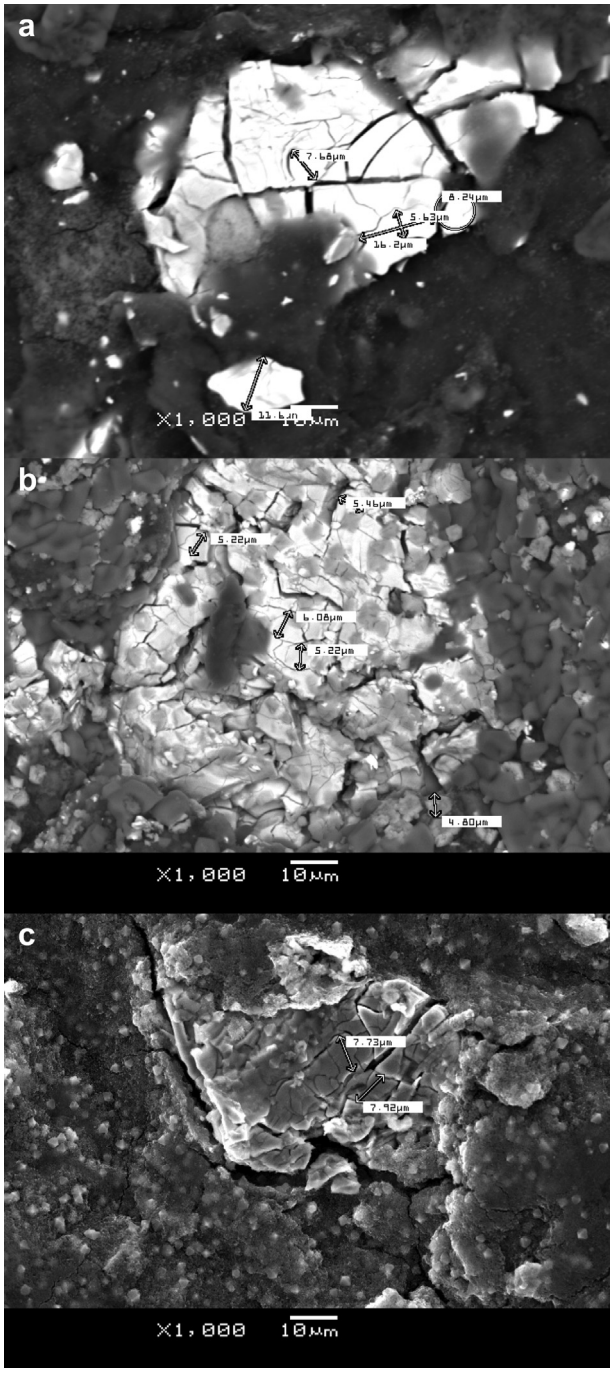

Fig. 6 – SEM micrographics for a. AB5M0, b. AB5M1 and c. AB5M2.

Charge transfer resistance (defined by the diameter of the semicircle) is greater for the sample AB5M0 than for the other studied alloys, resulting R_{ct}AB5M0 > R_{ct}AB5M2 > R_{ct}AB5M1.

This resistance does not show a linear trend in regard to the amount of molybdenum in the samples. The fact that the AB5M1 alloy depicts the lowest value of R_{ct} is also consistent with HRD results.

The alloy AB5M2 shows a better behavior at HRD experiments than AB5M0 although with lower capacity.

AB5M1 impedance is the smallest one. This fact can be associated with an increase in the active area or even an increase in the value of i_0 or both combined effects. In order to study the effect of these two parameters, SEM micrographics after activation processes were obtained. From these results we can perform an approximate determination of the particles mean radius value (ra). This parameter is inversely related to the active area (A_a) by volume unit according to the formula:

$$A_a = (3M)/(V_e \rho ra)$$

where M is the mass sample, V_e the electrode volume and ρ the sample density.

From the micrographics presented in Fig. 6, we can calculate ra concluding that AB5M1 mean radius is the smallest one. Calculated mean radius values are:

$$AB5M0/ra = 1.4 \times 10^{-3} cm$$

$$AB5M1/ra = 5 \times 10^{-4} cm$$

$$AB5M2/ra = 7.5 \times 10^{-4} cm$$

4. Conclusions

Three alloys have been synthesized by arc melting method. The incorporation of molybdenum induces contraction in the cell parameters of the crystalline structure of the studied alloys. This phenomenon is accompanied by a coexistence of two crystal structures, with general AB_5 and AB_3 stoichiometry.

The replacement of manganese by molybdenum, in the intermediate concentration tested (Mo 2% w/w) has a positive effect. The alloy corresponding to this concentration (AB5M1) presents the greatest discharge capacity; it presents the closest potential to system equilibrium potential and therefore the lowest overpotentials. This alloy also has the best behavior for HRD o high-rate dischargeability and in concordance, the lowest charge transfer resistance. This improvement is thought to be due to an increase in the active area.

Acknowledgment

The authors thank SNI and PDT and CSIC projects for the financial support. Dr. Zinola is a researcher at PEDECIBA/United Nations and a member of the Electrochemical Society. Dra. Díaz and Dr. Faccio are researchers at PEDECIBA/United Nations.

REFERENCES

[1] Zhang W, Visintin A, Srinivasan S, Appleby AJ, Lim HS. Investigation of changes in morphology and elemental distribution in metal hydride alloys after electrochemical cycling. J Power Sources 1998;75(1):84–9.

[2] Van Mal HH, Buschow KHJ, Miedema AR. Hydrogen absorption in $LaNi_5$ and related compounds: experimental observations and their explanation. J Less Common Met 1974;35(1):65–76.

[3] Anani A, Visintin A, Petrov K, Srinivasan S, Reilly J, Johnson J, et al. Alloys for hydrogen storage in nickel/hydrogen and nickel/metal hydride batteries. J Power Sources 1994;47(3):261–75.

[4] Zhao X, Ma Liqun. Recent progress in hydrogen storage alloys for nickel/metal hydride secondary batteries. Int J Hydrogen Energy 2009;3(11):4788–96.

[5] Mukerjee S, McBreen J, Marrero MR, Soriaga MP, Visintin A, Srinivasan S, et al. Effect of Zn additives to the electrolyte on the corrosion and cycle life of some AB_5H_x metal hydride electrodes. J Electrochem Soc 1997;144(9):258–61.

[6] Feng F, Geng M, Northwood DO. Electrochemical behaviour of intermetallic-based metal hydrides used in Ni/metal hydride (MH) batteries: a review. Int J Hydrogen Energy 2001;26(7):725–34.

[7] Zhang W, Kumar MP, Visintin A, Srinivasan S, Ploehn HJ. A microcalorimetric investigation of the thermodynamics and kinetics of hydriding–dehydriding reactions. J Alloys Compd 1996;242(1–2):143–52.

[8] Visintin A, Tori CA, Garaventta G, Triaca WE. The electrochemical performance of Pd-coated metal hydride electrodes with different binding additives in alkaline solution. J Electrochem Soc 1998;145(12):4169–72.

[9] Petrov K, Rostami A, Visintin A, Srinivasan S. Optimization of composition and structure of metal-hydride electrodes. J Electrochem Soc 1994;141(7):1747–50.

[10] Kim Dong-Myung, Jeon Seok-Won, Lee Jai-Young. A study of the development of a high capacity and high performance Zr–Ti–Mn–V–Ni hydrogen storage alloy for Ni–MH rechargeable batteries. J Alloys Compd 1998;279(2):209–14.

[11] Kim Dong-Myung, Lee Sang-Min, Jang Kuk-Jin, Lee Jai-Young. The electrode characteristics of over-stoichiometric $ZrMn_{0.5}V_{0.5}Ni_{1.4+y}$ ($y = 0.0$, 0.2, 0.4 and 0.6) alloys with C15 Laves phase structure. J Alloys Compd 1998;268(1–2):241–7.

[12] Klein B, Simon N, Klyamkine S, Latroche M, Percheron-Guégan A. Improvement of the thermodynamical and electrochemical properties of multicomponent Laves phase hydrides by thermal annealing. J Alloys Compd 1998;280(1–2):284–9.

[13] Sastri MVC, Viswanathan B, Srinivasa Murthy S. Metal hydrides. Fundamentals and applications. Berlin: Springer Verlag; 1998.

[14] Visintin A, Triaca WE, Arvia AJ, Peretti H, Bolcich JC, Zhang W, et al. Hydrogen energy progress XI. In: Veziroglu TN, Winter CJ, Baselt JP, Kreysa G, IAHE, editors. Proceedings of the 11th world hydrogen energy conference, Stuttgart, Germany, 23–28 June 1996, vol. 2; 1996. p. 1983.

[15] Peretti HA, Visintin A, Corso HL, Bonesi A, Triaca WE. In: Jornadas SAM 2000-IV Coloquio Latinoamericano de Fractura y Fatiga 2000. p. 1113.

[16] Young K, Ouchi T, Reichman B, Koch J, Fetcenko MA. Effects of Mo additive on the structure and electrochemical properties of low-temperature AB_5 metal hydride alloys. J Alloys Compd 2011;509(9):3995–4001.

[17] Kumar EA, Maiya MP, Murthy SS, Viswanathan B. Structural, hydrogen storage and thermodynamic properties of some mischmetal–nickel alloys with partial substitutions for nickel. J Alloys Compd 2009;476(1–2):92–7.

[18] Sato Y. Encyclopedia of electrochemical power sources. In: Secondary batteries – nickel systems: memory effect 2009. p. 534.

[19] An XH, Pan YB, Luo Q, Zhang X, Zhang YZ, Li Q. Application of a new kinetic model for the hydriding kinetics of $LaNi_{5-x}Al_x$ ($0 \le x \le 1.0$) alloys. J Alloys Compd 2010;506(1):63–9.

[20] Iosub V, Latroche M, Joubert J-M, Percheron-Guégan A. Optimisation of $MmNi_{5-x}Sn_x$ (Mm = La, Ce, Nd and Pr, $0.27 < x < 0.5$) compositions as hydrogen storage materials. Int J Hydrogen Energy 2006;31(1):101–8.

[21] Tliha M, Boussami S, Mathlouthi H, Lamloumi J, Percheron-Guégan A. Electrochemical characteristics of AB_5-type hydrogen storage alloys. J Alloys Compd 2010;506(2):559–64.

[22] Notten PHL, Hokkeling P. Double-phase hydride forming compounds: a new class of highly electrocatalytic materials. J Electrochem Soc 1991;138(7):1877–85.

[23] Tsuji Y, Yamamoto O, Yamamura Y, Seri H, Toyoguchi Y. US Patent 5,753,054; 1998.

[24] Senoh H, Hara Y, Inoue H, Iwakura C. Charge efficiency of misch metal-based hydrogen storage alloy electrodes at relatively low temperatures. Electrochim Acta 2001;46(7):967–71.

[25] Young K, Ouchi T, Huang B, Reichman B, Fetcenko MA. Studies of copper as a modifier in C14-predominant AB_2 metal hydride alloys. J Power Sources 2012;204:205–12.

[26] Iwakura C, Senoh H, Morimoto K, Hara Y, Inoue H. Influence of temperature on discharge process of misch metal-based hydrogen storage alloy electrodes. Electrochemistry 2002;70(1):2–7.

[27] Jakšić MM. Towards the reversible electrode for hydrogen evolution in industrially important electrochemical processes. Int J Hydrogen Energy 1986;11(8):519–32.

[28] Yeh MT, Beibutian VM, Hsu SE. Effect of Mo additive on hydrogen absorption of rare-earth based hydrogen storage alloy. J Alloys Compd 1999;293–295:721–3.

[29] Hsu SE, Beibutian VM, Yeh MT. Preparation of hydrogen storage alloys for applications of hydrogen storage and transportation. J Alloys Compd 2002;330–332:882–5.

[30] Ye H, Zhang H. Development of hydrogen-storage alloys for high-power nickel–metal hydride batteries. Adv Eng Mater 2001;3(7):481.

[31] Ye H, Zhang HJ. Grad Sch Chin Acad Sci 2003;20:381.

[32] Dong C. PowderX: Windows-95-based program for powder X-ray diffraction data processing. J Appl Cryst 1999;32(4):838.

[33] Boultif A, Louer D. Powder pattern indexing with the dichotomy method. J Appl Cryst 2004;37(5):724–31.

[34] Rietveld HM. A profile refinement method for nuclear and magnetic structures. J Appl Cryst 1969;2(2):65–71.

[35] Larson AC, Von Dreele RB. General structure analysis system (GSAS). Los Alamos National Laboratory Report LAUR; 2000. p. 86–748.

[36] Toby BH. EXPGUI, a graphical user interface for GSAS. J Appl Crystallogr 2001;34:210–3.

[37] Srivastavaa S, Upadhyay RK. Investigations of AB_5-type negative electrode for nickel-metal hydride cell with regard to electrochemical and microstructural characteristics. J Power Sources 2010;195(9):2996–3001.

[38] Díaz V, Teliz E, Ruiz F, Martinez PS, Zinola CF. Almacenamiento electroquímico de hidrógeno: efecto del molibdeno en las aleaciones metálicas formadoras de hidruros tipo AB5. Ingeniería Química 2013;42:14–8.

[39] Castro EB, Real SG, Bonesi A, Visintin A, Triaca WE. Electrochemical impedance characterization of porous metal hydride electrodes. Electrochim Acta 2004;49(22–23):3879–90.

[40] Visintin A, Castro EB, Real S, Triaca WE, Wang C, Soriaga MP. Electrochemical activation and electrocatalytic enhancement of a hydride-forming metal alloy modified with palladium, platinum and nickel. Electrochim Acta 2006;51(18):3658–67.